

# High-Resolution Spectroscopy of the Planetary Nebulae PM 1–242, PM 1–318 and PM 1–322

L. F. Miranda<sup>A,B,F</sup>, R. Vázquez<sup>C</sup>, M. A. Guerrero<sup>A</sup>, C. B. Pereira<sup>D</sup>,  
and E. Iñiguez-Garín<sup>C,E</sup>

<sup>A</sup> Instituto de Astrofísica de Andalucía – CSIC, Granada, Spain

<sup>B</sup> Facultade de Ciencias, Universidade de Vigo, Vigo, Spain

<sup>C</sup> Instituto de Astronomía, Universidad Nacional Autónoma de México, Ensenada, Mexico

<sup>D</sup> Observatorio Nacional – MCT, Rio de Janeiro, Brazil

<sup>E</sup> Facultad de Ciencias, Universidad Autónoma de Baja California, Ensenada, Mexico

<sup>F</sup> Corresponding author. Email: lfm@iaa.es

Received 2009 June 29, accepted 2010 April 23

**Abstract:** We have recently confirmed the planetary nebula (PN) nature of PM 1–242, PM 1–318 and PM 1–322. Here we present high-resolution long-slit spectra of these three PNe in order to analyze their internal kinematics and to investigate their physical structure. PM 1–242 is a tilted ring and not an elliptical PN as suggested by direct images. The object is probably related to ring-like PNe and shows an unusual point-symmetric brightness distribution in the ring. PM 1–318 is a pole-on elliptical PN, instead of a circular one as suggested by direct images. PM 1–322 is spatially unresolved and its spectrum shows large differences between the forbidden lines and H $\alpha$  profiles, with the latter showing a double-peaked profile and relatively extended wings (FWZI  $\sim 325$  km s<sup>-1</sup>). These properties are found in other PNe that are suspected to host a symbiotic central star.

**Keywords:** circumstellar matter — ISM: jets and outflows — planetary nebulae: individual (PM 1–242, PM 1–318, PM 1–322)

## 1 Introduction

Planetary nebulae (PNe) evolve from Asymptotic Giant Branch (AGB) stars after a short post-AGB transition and represent the last evolutionary stage of solar-type stars ( $M \leq 8 M_{\odot}$ ) before the white dwarf phase (Bloeker 1995). The transformation of an AGB star into a PN involves a dramatic change in all stellar and circumstellar properties (Balick & Frank 2002). In particular, while mass ejection in the AGB phase is spherical, the PN phase is dominated by axisymmetric shells, peculiar envelope geometries and collimated outflows (Manchado et al. 1996; Miranda, Ramos-Larios & Guerrero 2010). Direct images allow us to study the morphology of PNe and to identify the structural components present in these objects. However, the study of the internal kinematics of PNe is crucial to understand the nature of the components observed in the images, to determine their physical structure, and to investigate the ejection processes involved in their formation (e.g. Miranda, Guerrero & Torrelles 1999).

We have started an intermediate-resolution spectroscopic program to establish the true nature of sources classified as post-AGB star and PN candidates on the basis of their IRAS colours. Among other results (see Pereira & Miranda 2007), we have confirmed the PN nature of several objects and analyzed their morphology (Pereira & Miranda 2005; Miranda, Pereira & Guerrero 2009, hereafter MPG09).

In this paper we present high-resolution long-slit spectra of three of these confirmed PNe: PM 1–242, PM 1–318 and PM 1–322. The spectra allow us to analyze their internal kinematics and to investigate their physical structure. At least in two objects, the real structure derived from the long-slit spectra differs from that suggested by the morphology observed in direct images.

## 2 Observations

High-resolution long-slit spectra were obtained using the Manchester Echelle Spectrometer (MES) at the 2.1-m telescope on San Pedro Mártir Observatory (Mexico) on 2007, July 16–20. A Site CCD with  $1024 \times 1024$  pixels was used as detector. In the case of PM 1–242 a spectrum in the H $\alpha$  and [NII]  $\lambda$  6584 (hereafter [NII]) lines was obtained with the slit oriented at position angle (PA)  $90^{\circ}$ , an exposure time of 900 s and a  $2 \times 2$  binning on the detector. For PM 1–318, the [OIII]  $\lambda$  5007 (hereafter [OIII]) line was observed with the slit oriented at PA  $315^{\circ}$ , an exposure time of 1800 s and without binning. Finally, in the case of PM 1–322, the H $\alpha$ , [NII] and [OIII] lines were observed with the slit oriented at PA  $120^{\circ}$ , an exposure time of 1800 s and without binning. A slit width of  $1.6''$  was used in all cases. The long-slit spectra were flat fielded, bias corrected and, finally, wavelength calibrated with a Th-Ar lamp to an accuracy of  $\pm 1$  km s<sup>-1</sup>, using standard routines for long-slit spectroscopy within the IRAF package.

The spectral resolution, determined by the FWHM of the Th-Ar comparison lines, is  $\simeq 12 \text{ km s}^{-1}$ . The spatial resolution, determined by the seeing, is  $1' - 1.5''$ .

### 3 Results and Discussion

In the following, we will present and discuss the results obtained for the three PNe. A brief description of their morphology and spectral properties is also provided from the previous results by Pereira & Miranda (2005) and MPG09.

#### 3.1 PM 1–242 (IRAS 18320+0005)

PM 1–242 is a medium-to-high excitation PN with relatively strong  $\text{He II}$  emission and relatively weak  $[\text{N II}]$  and  $[\text{S II}]$  emissions (see MPG09). Figure 1 shows the  $[\text{N II}]$  image of PM 1–242 presented by MPG09. Morphologically, PM 1–242 can be classified as an elliptical PN with its major axis along the north-south direction and a size of  $\simeq 8'' \times 5''$ . Two bright low-excitation, point-symmetric arcs trace the ellipse. Faint protrusions and/or knots are observed along PAs  $50^\circ$ ,  $225^\circ$  and  $230^\circ$ , particularly in  $\text{H}\alpha$  and  $[\text{O III}]$  (see MPG09). As mentioned by MPG09, the images do not allow us to determine whether PM 1–242 is an ellipsoid containing two point-symmetric arcs, with the major axis along the north-south direction, or a bipolar PN with a bright ring, faint bipolar extensions represented by the protrusions/knots and with the major axis along the east-west direction.

A position-velocity (PV) map of the  $[\text{N II}]$  line derived from the long-slit spectrum is also shown in Figure 1. The PV map of the  $\text{H}\alpha$  line (not shown here) is qualitatively similar to the  $[\text{N II}]$  one. The PV maps show two velocity components separated  $\simeq 36$  and  $\simeq 42 \text{ km s}^{-1}$  in  $\text{H}\alpha$  and  $[\text{N II}]$ , respectively. The two components correspond to emission from the arcs at the minor axis of the ellipse (Figure 1). In particular, the blueshifted bright component corresponds to a bright knot at the eastern edge of the ellipse while the redshifted faint component corresponds to a faint knot at the western edge. From the center of the  $\text{H}\alpha$  and  $[\text{N II}]$  emission features in the PV maps we derive a heliocentric systemic velocity of  $\simeq +72.6 \text{ km s}^{-1}$ .

The presence of two velocity components at different velocities is not compatible with the slit being oriented along the minor axis of an ellipsoid. If this were the case, one would expect the two components to be located at the systemic velocity. On the contrary, the results strongly suggest that the observed ellipse is a tilted ring with its polar axis oriented along the east-west direction. The ring is tilted so that its eastern side points toward the observer and its western side recedes away. Assuming that the ring is circular, we derive an inclination angle of  $\simeq 30^\circ$  for its polar axis with respect to the observer. Taking into account this angle, the expansion velocity of the ring is  $\simeq 20$  and  $\simeq 25 \text{ km s}^{-1}$  in  $\text{H}\alpha$  and  $[\text{N II}]$ , respectively.

These results show that the main structure of PM 1–242 is a tilted ring. The faint protrusions and knots (see MPG09) suggest that faint bipolar lobes may also be present and, hence, PM 1–242 could be a bipolar PN, although the presence of faint lobes needs to be confirmed

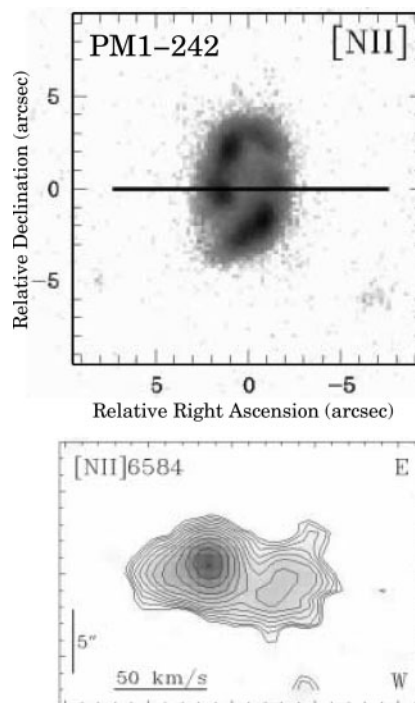


**Figure 1** **Top:**  $[\text{N II}] \lambda 6584$  image of PM 1–242 (adapted from MPG09). The slit position used for high resolution spectroscopy is indicated. **Bottom:** Grey-scale and contours position-velocity map of the  $[\text{N II}]$  emission line derived from the long-slit spectrum. The orientation (E-W) and the spatial and velocity scales are indicated.

by deeper observations. In any case, PM 1–242 is probably related to ring-like PNe like, e.g. IC 2149 (Vázquez et al. 1999), Me 1-1 (Pereira et al. 2008), WeBo 1 (Bond, Pollacco & Webbink 2003) and SuWt 2 (Jones et al. 2010). In these PNe, a bright ring is the dominant structure in the nebula, which is, in some cases, accompanied by very faint bipolar lobes. Particularly interesting in PM 1–242 is the point-symmetric brightness distribution in the ring. Point-symmetry is usually observed in the lobes of bipolar PNe or in collimated structures usually associated to these objects, but to the best of our knowledge PM 1–242 is the only PN that shows this characteristic in the equatorial structure.

#### 3.2 PM 1–318 (IRAS 20077+3722)

PM 1–318 is a high-excitation PN with strong  $\text{He II}$  lines (e.g.  $\text{He II} \lambda 4686/\text{H}\beta \simeq 1$ ) and extremely weak or absent low-excitation emission lines (MPG09). The  $[\text{O III}]$  image of PM 1–318 by MPG09, reproduced in Figure 2, shows that the nebula consists of an inner ring-like shell with two enhanced opposite regions, surrounded by a faint, round attached shell. The morphology observed in the images classifies PM 1–318 as a round PN.

A PV map of the  $[\text{O III}]$  emission line is also presented in Figure 2. The  $[\text{O III}]$  emission feature corresponds to emission from the inner shell because the spectrum is not deep enough to detect the faint outer shell. The  $[\text{O III}]$  emission feature appears as a tilted velocity ellipse on the PV map. The southeastern nebular regions are blueshifted

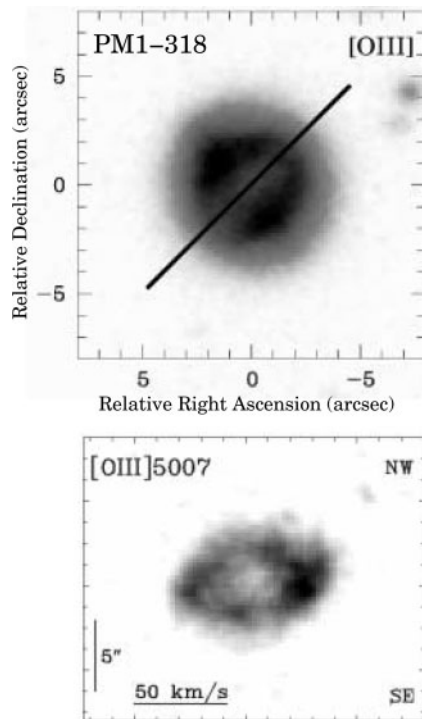


**Figure 2** **Top:** [OIII]  $\lambda$  5007 image of PM 1–318 (adapted from MPG09). The slit position used for high resolution spectroscopy is indicated. **Bottom:** Grey-scale position-velocity map of the [OIII] emission line derived from the long-slit spectrum. The orientation (NW–SE) and the spatial and velocity scales are indicated.

while the northwestern nebular regions are redshifted. A velocity splitting of  $\simeq 60 \text{ km s}^{-1}$  is measured at the center of the emission feature and a heliocentric systemic velocity of  $\simeq -99 \text{ km s}^{-1}$  is derived from that center. We note that radial velocities up to  $\simeq \pm 40 \text{ km s}^{-1}$  from the systemic velocity are observed. The inner regions of the velocity ellipse show a decreasing [OIII] intensity, which suggests that the [OIII] emission mainly originates in a relatively thin layer of the inner shell, as also suggested by the direct image.

The tilt of the velocity ellipse on the PV map rules out that the inner shell of PM 1–318 is spherical (or round) because, in this case, the velocity ellipse would not be tilted on the PV map. This result strongly suggests that the inner shell is an ellipsoid with the major axis tilted with respect to the observer and oriented near PA  $315^\circ$ . Moreover, the largest velocities in the velocity ellipse are observed almost along the line of sight to the center of the nebula. This implies a relatively small inclination angle of the polar axis with respect to the observer and, hence, a polar expansion velocity of the order of  $\sim 30\text{--}40 \text{ km s}^{-1}$ . From these results we conclude that PM 1–318 is an (almost) pole-on elliptical PN. The enhanced regions in the inner shell probably represent a bright equatorial region in the ellipsoid.

### 3.3 PM 1–322 (IRAS 20124+5844)

PM 1–322 was identified as a new PN by Pereira & Miranda (2005). It exhibits very strong [OIII]  $\lambda$  4363 line

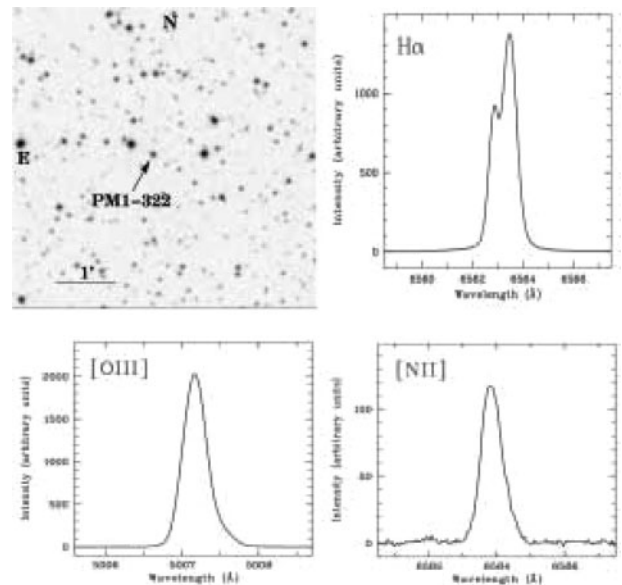


**Figure 3** Line profiles of the H $\alpha$ , [NII] and [OIII] emission lines in PM 1–322. An identification chart obtained from the POSS is also shown (upper left).

emission ([OIII]  $\lambda$  4363/H $\beta$   $\simeq 1.2$ ) indicating a high electron density ( $\geq 10^6 \text{ cm}^{-3}$ ). The nebula is unresolved in our direct images. The compactness and high electron density suggest that PM 1–322 is a very young PN. On the other hand, these properties and the position of PM 1–322 in the [OIII]  $\lambda$  4363/H $\gamma$  versus [OIII]  $\lambda$  5007/H $\beta$  diagram indicate that PM 1–322 could be a symbiotic star (Pereira & Miranda 2005).

PM 1–322 is also spatially unresolved in the long-slit spectra. Therefore, we show in Figure 3 the H $\alpha$ , [NII] and [OIII] emission line profiles derived from the spectra. The [NII] and [OIII] profiles presents a single peak at a heliocentric radial velocity of  $\simeq +27.2 \text{ km s}^{-1}$  that can be considered as the systemic velocity of the nebula. The FWHM (corrected of instrumental resolution) of the [NII] and [OIII] profiles is  $\simeq 30$  and  $\simeq 18 \text{ km s}^{-1}$ , respectively. The H $\alpha$  emission line shows a double-peaked profile. The heliocentric radial velocity derived from the centroid of the H $\alpha$  profile is  $\simeq +27.2 \text{ km s}^{-1}$ , in excellent agreement with the systemic velocity of PM 1–322 derived from the forbidden lines. The two emission peaks of the H $\alpha$  profile are observed at  $-17.5$  and  $+9 \text{ km s}^{-1}$  with respect to the systemic velocity and the red peak is stronger than the blue one. The emission peaks are separated by an apparent ‘absorption reversal’ that is blueshifted by  $-9.6 \text{ km s}^{-1}$  with respect to the systemic velocity. Finally, the wings of the H $\alpha$  line can be traced up to  $\simeq 325 \text{ km s}^{-1}$  (FWZI) while the [NII] and [OIII] lines present a much smaller FWZI of  $\simeq 90 \text{ km s}^{-1}$ .

The large differences between the forbidden lines and H $\alpha$  profiles suggest a different origin for these emissions. Given the high density in the object, the regions probed via the H $\alpha$  emission may critically depend upon the density and its variation within the object. Therefore, the H $\alpha$  emission may be produced in regions that do not contribute

to [NII] and [OIII] emissions. In particular, the relatively large wings of the H $\alpha$  emission could be due to Rayleigh-Raman scattering in a very dense region close to the central star (see Lee & Hyung 2000). The spectral properties of PM 1–322 are remarkably similar to these found in other PNe suspected to host a symbiotic central star. These PNe are characterized by differences between the forbidden lines and H $\alpha$  profiles, a double-peaked H $\alpha$  profile, with very similar properties to these observed in PM 1–322, and extended H $\alpha$  wings (e.g. Balick 1989; Miranda, Torrelles & Eiroa 1996; Guerrero et al. 2001; Arrieta & Torres-Peimbert 2003). These results reinforce the idea that the central star of PM 1–322 is a symbiotic star.

### 3.4 Conclusions

We have presented high-resolution long-slit spectra of three new confirmed PNe: PM 1–242, PM 1–318 and PM 1–322 with the aim of investigating their internal kinematics and physical structure. The main conclusion of this work can be summarized as follows:

- PM 1–242 is a ring-like PN, but not an elliptical PN as suggested by direct images. Interestingly, the ring displays a point-symmetric brightness distribution which is unusual among ring-like PNe and bipolar PNe with central rings.
- PM 1–318 is an almost pole-on elliptical PN with an enhanced equatorial region, but not a round PN as suggested by direct images.
- PM 1–322 is spatially unresolved and presents large differences between the forbidden lines and H $\alpha$  profiles, a double-peaked H $\alpha$  profile and relatively extended H $\alpha$  wings. These characteristics are also found in other PNe believed to host symbiotic central stars.

### Acknowledgments

This work has been supported partially by grants AYA2005-01495 of the Spanish MEC, and AYA2008-01934 of the Spanish MICINN, by grant FQM1747 of Consejería de Innovación, Ciencia y Empresa of Junta de Andalucía, and by CONACYT grant 102582 and PAPIIT-UNAM grant IN109509 (Mexico).

### References

- Arrieta, A. & Torres-Peimbert, S., 2003, *ApJS*, 147, 97  
 Balick, B., 1989, *AJ*, 97, 476  
 Balick, B. & Frank, A., 2002, *ARA&A*, 40, 439  
 Bloeker, T., 1995, *A&A*, 299, 755  
 Bond, H. E., Pollacco, D. L. & Webbink, R. F., 2003, *AJ*, 125, 260  
 Doyle, S., Balick, B., Corradi, R. L. M. & Schwarz, H. E., 2000, *AJ*, 119, 1339  
 Guerrero, M. A., Miranda, L. F., Chu, Y.-H., Rodríguez, M. & Williams, R. M., 2001, *ApJ*, 563, 883  
 Jones, D., Lloyd, M., Mitchell, D. L., Pollacco, D. L., O'Brien, T. J. & Vaytet, N. M. H., 2010, *MNRAS*, 401, 405  
 Lee, H.-W. & Hyung, S., 2000, *ApJ*, 530, L49  
 Manchado, A., Guerrero, M. A., Stanghellini, L. & Serra-Ricart, M., 1996, *The IAC Morphological Catalog of Northern Galactic Planetary Nebulae (La Laguna: Instituto de Astrofísica de Canarias)*  
 Miranda, L. F., Guerrero, M. A. & Torrelles, J. M., 1999, *AJ*, 117, 1421  
 Miranda, L. F., Pereira, C. B. & Guerrero, M. A., 2009, *AJ*, 137, 4140  
 Miranda, L. F., Torrelles, J. M. & Eiroa, C., 1996, *ApJ*, 461, L111  
 Miranda, L. F., Ramos-Larios, G. & Guerrero, M. A., 2010, *PASA*, 27, 180  
 Pereira, C. B. & Miranda, L. F., 2005, *A&A*, 433, 579  
 Pereira, C. B. & Miranda, L. F., 2007, *A&A*, 462, 231  
 Pereira, C. B., Miranda, L. F., Smith, V. V. & Cunha, K., 2008, *A&A*, 477, 535  
 Vázquez, R. et al., 2002, *ApJ*, 576, 860